

On-device Scalable Image-based Localization

Ngoc-Trung Tran, Dang-Khoa Le Tan, Anh-Dzung Doan, Thanh-Toan Do, Tuan-Anh Bui, Ngai-Man Cheung

Abstract—We present the scalable design of an entire on-device system for large-scale urban localization. The proposed design integrates compact image retrieval and 2D-3D correspondence search to estimate the camera pose in a city region of extensive coverage. Our design is GPS agnostic and does not require the network connection. The system explores the use of an abundant dataset: Google Street View (GSV). In order to overcome the resource constraints of mobile devices, we carefully optimize the system design at every stage: we use state-of-the-art image retrieval to quickly locate candidate regions and limit candidate 3D points; we propose a new hashing-based approach for fast computation of 2D-3D correspondences and new one-many RANSAC for accurate pose estimation. The experiments are conducted on benchmark datasets for 2D-3D correspondence search and on a database of over 227K Google Street View (GSV) images for the overall system. Results show that our 2D-3D correspondence search achieves state-of-the-art performance on some benchmark datasets and our system can accurately and quickly localize mobile images; the median error is less than 4 meters and the processing time is averagely less than 10s on a typical mobile device.

Index Terms—Large-scale image-based localization, on-device localization, 2D-3D correspondence search, 2D-3D matching, RANSAC.

I. INTRODUCTION

ESTIMATING accurately the absolute camera pose (with respect to a real-world coordinate) is a fundamental problem of many applications: robotics, augmented reality, autonomous vehicle navigation, location recognition, etc... Using visual/image sensors (e.g., camera) are often the first consideration to develop such localization system because it provides more information about the scene structure than other sensors. Then, sensors data such as GPS (Global Positioning System), WiFi, Bluetooth are used to support/simplify the localization. However, the accuracy of embedded GPS sensors in devices highly depends on the surrounding environments. The GPS-based location performs poorly in downtown areas and urban canyons, e.g., the localization error is up to 100m or more [26]. Moreover, the GPS information is sometimes not available for indoor. The GPS is also sensitive to magnetic disturbances and can be denied/lost or easily hacked, which is not suitable for high-security robots. WiFi/Bluetooth can be also used for localization, but they are not always available

for outdoor. Thus, it is necessary to build an entirely on-device image-based localization system without the support of GPS/Bluetooth/WiFi.

State-of-the-art methods for image-based localization [1], [2], [3] assume the existence of 3D scene models. The 3D models are often pre-built from image datasets by using advanced techniques of Structure-from-Motion (SfM) [4]. While such methods are suitable for powerful machines (workstation/servers), they are difficult to be employed on mobile devices due to the resource constraints of the devices. Current solutions for the location using mobile devices are to confine to small areas [5] or require back-end supports [6], [7], [8]. Compressing schemes [9], [10] can also be considered [11] but the issue still remains when the map grows. Alternatively, partitioning data/models into smaller parts, and manipulating only one part at a time is a scalable approach. However, determining the appropriate parts usually require GPS/WiFi or manual inputs [12].

In this paper, we investigate entirely on-device large-scale urban localization, e.g. we can localize the camera position in the real-world environment. Specifically, at first, in order to overcome on-device resource constraints for the large-scale problem, we propose a design that integrates a compact image retrieval and 2D-3D correspondence search methods. In particular, we partition the whole scene into segments to build a set of sub-3D models. Given a query, we use image retrieval to quickly identify the coarse locations (sub-3D models). Then, we perform 2D-3D correspondences search between the query image and the selected sub-models. This design allows us to load only a sub-model into RAM for processing and reduce the memory and computation requirement. We show that with this design, it is feasible to enlarge the map.

Secondly, we address the localization problem by relaxing the test ratio to have more tentative matches (multiple matches per query descriptor), and we propose a RANSAC-based solution detect inliers from a large number of matches in low-computational complexity. Before of that, in order to seek multiple matches efficiently, we propose an efficient 2D-3D correspondence search method based on coarse-to-fine search scheme with a simple prioritizing scheme. We improve localization performance on two both aspects: 2D-3D matching and pose estimation. Our goal is to develop a practical localization method that achieves better trade-off among complexity, memory, and accuracy. We demonstrate our method on benchmark datasets of millions of 3D points. The results show our method is faster than most of the previous works and achieves the competitive accuracy. To the best of our knowledge, we are the first work confirms that using compressed descriptors can still potentially achieves state-of-the-art performance on benchmark datasets of large-scale

Ngoc-Trung Tran, Dang-Khoa Le Tan, Anh-Dzung Doan, Anh-Tuan Bui and Ngai-Man Cheung are with the Singapore University of Technology and Design, Singapore.

E-mail: ngoctrung_tran@sutd.edu.sg

E-mail: letandang_khoa@sutd.edu.sg

E-mail: anhdung_doan@sutd.edu.sg

E-mail: tuananh_bui@sutd.edu.sg

E-mail: ngaiman_cheung@sutd.edu.sg

Thanh-Toan Do is with the University of Adelaide, Australia.

E-mail: thanh-toan.do@adelaide.edu.au

image-based localization. It's worth noting that although some minor parts of our system were separately proposed in some previous works. Our novelty is the entire system, which is careful-designed and unique. In addition, our method can achieve better requirements (memory and computation) than state-of-the-art methods, as well as competitive accuracy.

Finally, we demonstrate our system on street view images of Google Street View (GSV) [13]. GSV is an abundant source of street-view images acquired over many streets around the world. Our goal is to investigate the potential of using GSV dataset to compute full camera pose (3D position and orientation), which is interesting for practical localization systems. While there exists a number of prior works building their systems on GSV [14], [15], [16], [17], our work is different and focuses on estimation of camera pose in a large-scale dataset using a mobile device. Note that pose estimation using GSV images is challenging: low sampling rate, distortion, co-linear cameras, wide baseline, or obstacle objects like tree or vehicles, while query images are taken under different devices, timing and conditions (distortion, illumination, ...). However, leveraging GSV is potentially a practical approach since being able to expand the system coverage to any cities on the world without spending many efforts for data collection.

II. RELATED WORKS

A. Image based Localization

Early works of image-based localization can be divided into two categories: retrieval based approach and 3D model-based approach (or direct search approach). Retrieval based methods [18], [19], [20], [14] are closely related to image retrieval by matching query features against geo-tagged database images to find a set of similar ones. The query pose can be inferred from those references. This approach highly depends on image retrieval and does not get the benefit of 3D scene structure. Otherwise, the model-based approach directly performs the 2D-3D matching between 2D features of the query image and 3D points of the 3D model. A 3D model is a set of 3D points, given a set of images, the 3D point cloud is built from the images by using modern Structure-from-Motion (SfM) approaches e.g. [4]. This approach achieves better results than image retrieval based one as it imposes stronger geometric constraints. Preferably, it tells more information about the 3D structure of the scene. The camera pose can then be computed from 2D-3D correspondences by RANSAC within DLT inside.

The representative works of 3D model based approach are [21], [9], [22], [23], [1]. [21] use SfM models as the basis for localization. First, it performs image retrieval and then computes 2D-3D matches between 2D features in the query against 3D points visible in top retrieved images. Synthetic views of 3D points are generated to improve image registration. [9] compress the 3D model and prioritize 3D points (given the prior knowledge from visibility graph) in 3D-2D correspondence search that allows the "common" views to be localized quickly. [22] propose the efficient prioritization scheme which is able to early stop the 2D-3D direct search. [23], [1] propose two-directional searches from 2D image features to 3D points and vice versa, which can recover some lost matches due to ratio test.

A recent trend in localization shifts the task of finding correct correspondences from matching step to pose estimation step, by leverage geometric cues. [2] propose an outliers filter with the assumption of a known direction of gravitational vector and the rough estimate of the ground plane in a 3D model. Consequently, the pose estimation problem can be cast into a 2D registration problem. Follow the same setup as [2], [24] propose a filtering strategy based on Hough voting in linear complexity. In order to accelerate the method, they exploit the local feature geometry based verification, e.g. the viewing direction constraints, or the scale and orientation of 2D local features to early reject false matches before voting.

B. On-device systems

All aforementioned 3D model-based methods require a large amount of memory for SIFT descriptors. For on-device point-of-view, loading a single, large 3D model on memory to perform the correspondence search is impractical. Some earlier works tried to build localization systems running on mobile devices. [12] keep the 3D model out-of-core and manually divide it into multiple segments that fit into the memory capability of a mobile phone. The work is confined to small workspaces and requires the initial location, such as WiFi, GPS,... or manual inputs provided. The work is extended for outdoor localization [6], but still, need prior knowledge of coarse location, and wireless network to download relevant portions of pre-partitioned databases. [7] and [8] employ the client-server architectures. Pose tracking is employed on devices and its pose is corrected by matching to global model to avoid the drift. While [7] need to keep a part of global model locally to obtain fast tracking and use intensive SIFT descriptors, [8] construct their own local map of the environment and using global results received from an external server to align this map. [5] use Harris corner detectors and extract two binary features for tracking and 2D-3D matching. It avoids wasting computation by performing matching over only a small batch of tracked keypoints. [11] implemented a fast pose estimation and tracking via entirely on a device. It uses Inverted Multi-Index (IMI) [25] for indexing, its 3D models are also compressed before to fit into device memory. However, using this scheme may remove important 3D points, and lead to fewer matches that is insufficient to localize many queries.

C. Using Street View images for localization

One of the difficulties in developing a large-scale image-based localization is data collection, which requires ground-truth data, e.g. GPS, in real-world. Several on-device systems [6], [7], [8], [5], [11] have to collect their own dataset for experiments which are usually confined to small areas. Mining images from online photo collections like Flickr [4] is an attractive solution. However, this undertaking is challenging due to poor labels, noisy distortions to be distributed in the real world. Also, the coverage of images is often popular places, e.g. city landmarks. [26] approached by using camera-mounted surveying vehicles to harness the street-level data in San Francisco. They published a dataset containing 150k

high-resolution panoramic images of San Francisco to the community. [14] use GSV images to localize UAV by generating virtual views and matching images with strong viewpoint changes. [16] perform tracking the vehicles inside the structure of street-view graph by a Bayesian framework. This system requires compasses measurements, fixed cameras within many assumptions of video capturing conditions. [17] track the pose of a camera from a short stream of images and geo-register the camera by including GSV images into the local reconstruction of the image stream. Nearby panoramic images determined by image retrieval with restricts of locations inferred by GPS or cellular networks in surrounding 1km area.

III. PROPOSED SYSTEM

We first provide an overview of our proposed on-device localization system. Then, we discuss 2D-3D correspondence search, which is our main contribution.

A. On-device localization system

Our proposed system design aims to: i) leverage a large collection of GSV images for urban localization; ii) overcome the constraints of memory and computation when using a large-scale dataset on a typical mobile device. The input of our system is a query image taken by user's camera. The output is the real-world GPS location. Our system has three main components (Fig. 1): a set of 3D reconstruction models to represent the scene, an image retrieval system to identify 3D models for pose estimation, and a system to compute correspondences between 2D features and 3D points (Section III-B). In this work, our choice of image retrieval, a state-of-the-art method [27], is for memory-efficiency, good accuracy, and fast indexing. It aims to demonstrate the possibility of our system design. We then focus more on improving localization part to reduce its latency and to get our on-device system work more practical. Note that deciding which features are used for the system is hard (to trade-off memory, computation, and accuracy), and it is beyond the scope of this paper. We choose SIFT [28] features as the input for both image retrieval and 2D-3D correspondence search, simply because its reliability and efficiency have been demonstrated in the literature of those two fields. Though the same pipeline can be exactly applied to other kinds of features.

1) *Dataset*: We collect GSV images at a resolution of 640×640 pixels. These images have exact GPS. We collect images that cover city regions in Singapore. At each Street View *place mark* (a spot on the street), the 360-degree spherical view is sampled by 20 rectilinear view images (18° interval between two consecutive side view images) at 3 different elevations (5° , 15° and 30°). Each rectilinear view has 90° field-of-view and is considered a pinhole camera (Fig. 2). Therefore, 60 images are sampled per placemark. The distance between two placemarks is about 10-12m. We also collect 576 query images with the accurate GPS ground-truth position. Note that these query images are captured using different devices and under different conditions from that of GSV. See our dataset and query examples in Figures 4 and 5. Our dataset covers about 15km road distance shown in Fig. 3.

2) *Scene representation using small 3D models*: Constructing a single, large 3D model from a large-scale dataset is computationally expensive. Moreover, it could be difficult to load the 3D model into the RAM of mobile devices. In addition, representing the scene by a single model is inflexible: It is rather difficult to update a large model when some region of the city changes (e.g. newly constructed buildings). Therefore, in our work, we divide the scene into small *segments* and build small 3D models for individual segments (Fig. 6). Reconstruction of small 3D models can be performed in parallel, and this reduces the processing time to build the scene models. Moreover, provided that the correct small 3D models can be identified, localization using small 3D models can achieve better accuracy as there is less number of distracting 3D points. Furthermore, localization time can be reduced using small 3D models. We use 8-10 consecutive GSV placemarks to define a segment of the scene. As we sample 60 street view images per placemark, there are 480-600 images for a segment. We use Incremental SfM [4], [29] to reconstruct a 3D model from the images of a segment. See examples of our 3D models in Fig. 7.

Overlapping of segments: We investigate overlapping between two consecutive segments. This is to ensure accurate localization for query images capturing buildings at the segment boundaries. We conducted an experiment to evaluate the localization accuracy at zero, two and four place marks overlapped. In this experiment, we used image retrieval to find the 20 or 50 top similar database images, given a query image. Results in Fig. 8 suggest that with segments overlapped at two placemarks can ensure good localization accuracy. Note that the extent of overlapping is a trade-off between accuracy and storage. Besides, a retrieved list of 20 database images achieves good accuracy-speed trade-off.

Coverage of each segment: As the coverage (size) of each segment increases, the percentage of overlapped place marks decreases and hence storage (3D points) redundancy decreases. However, the localization accuracy decreases as the segment coverage increases, because there are more distracting 3D points in a 3D model. We conducted an experiment to determine an appropriate segment size: We reconstructed a 3D model from a number of images: 480-600 images (8-10 placemarks), 660-840 images (11-14 placemarks), and 1200-1500 images (20-25 placemarks). We applied the state of the art method, Active Correspondence Search (ACS) [23], to compute the localization accuracy using the 3D model. Table I shows the results, which suggest that using segment with 8-10 placemarks achieves the best accuracy. The localization accuracy degrades rapidly as we increase the segment coverage for GSV dataset. Therefore, in our system, we use 8-10 consecutive GSV placemarks to define a segment. Although [12] has also proposed to divide a scene into multiple segments, their these design parameters have not been studied. Moreover, its design is not memory-efficient and just in a small workspace. It also requires prior additional sensor data, e.g. GPS, WiFi to determine the search region. In addition, this work requires manual steps, e.g. registering individual models into a single global coordinate. On the other hand, our models are automatically reconstructed or registered, and our system

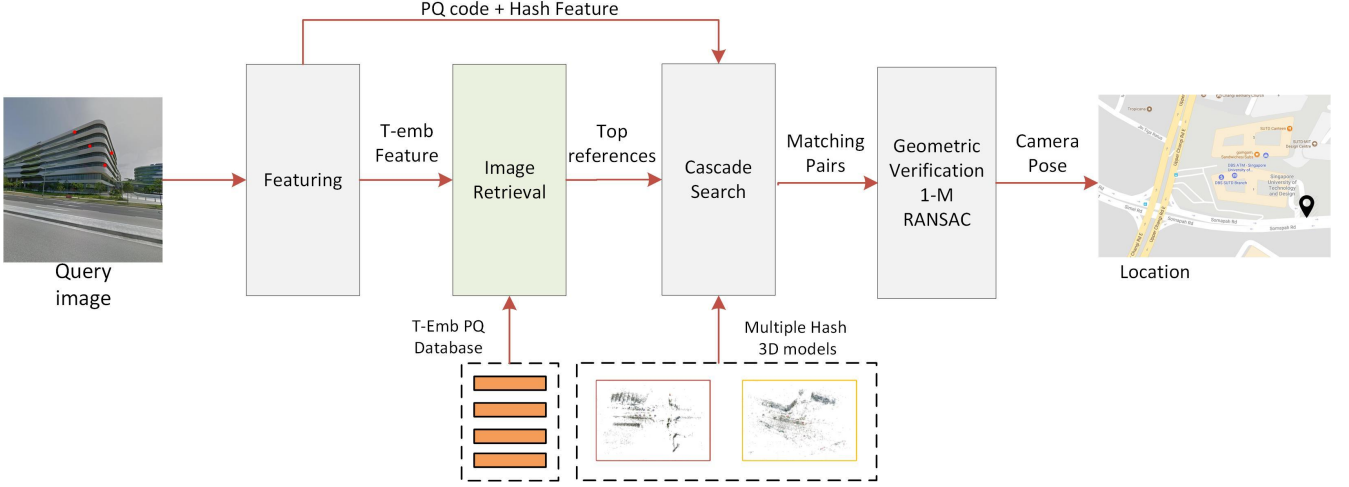


Fig. 1. Overview of our proposed system. Image retrieval (IR) identifies reference images similar to the query image. The reference images returned by IR indicate 3D models for use in camera pose estimation.



Fig. 2. A panoramic image and its rectilinear views.

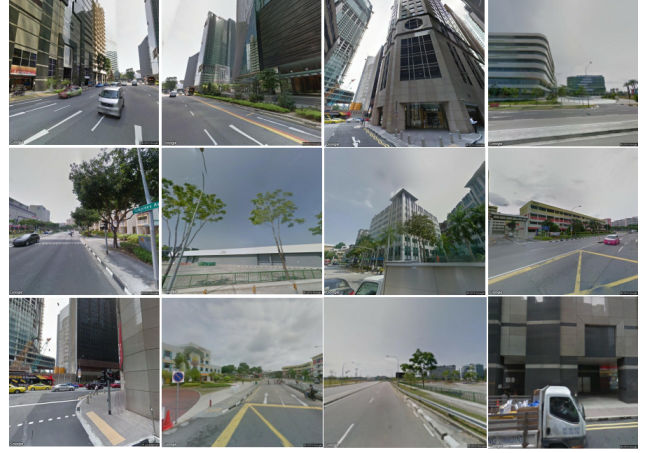


Fig. 4. Examples of GSV images.

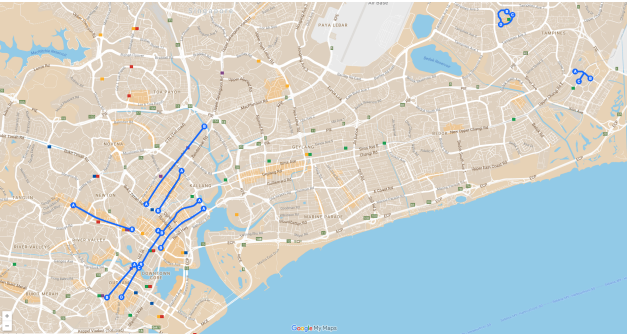


Fig. 3. The coverage of our 200K dataset taking over about 15km road distance (roads marked by blue lines).



Fig. 5. Examples of query images.

can localize entirely on a mobile device at large scale.

3) *Model indexing by image retrieval*: We also use image retrieval (IR) in our framework but in contrast to the image retrieval based approach that infers the query pose from the top list of similar images. The localization is sensitive to the resulted list. In our case, we use IR to identify the list of 3D models \mathbb{M}_i for localizing the query image. IR serves as search

TABLE I
THE EFFECT OF SEGMENT SIZE ON THE LOCALIZATION ACCURACY.

#Place marks	#Images	% of #queries with error $\leq 5m$
8-10	480-600	90%
11-14	660-840	80%
20-25	1200-1500	60%

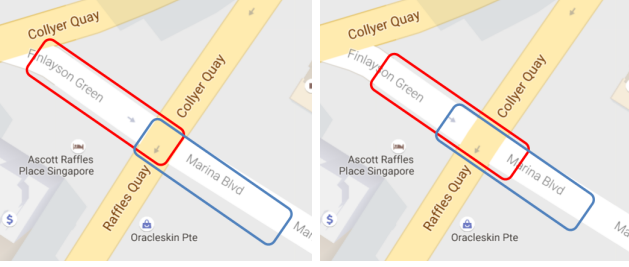


Fig. 6. We represent the scene with overlapping segments, and build small 3D models for individual segments. We investigate the effect of overlapping on localization accuracy.

coarse to limit the searching space for the second step.

Let $\{I_j\}_{j=1:N}$ be the N images in dataset. If the image I_j was used to reconstruct 3D model \mathbb{M}_i , we set $r(\mathbb{M}_i, I_j) = 1$, otherwise $r(\mathbb{M}_i, I_j) = 0$. Given a query image I_q , image retrieval seeks top N_t similar images from the dataset, namely $I_{j_1}, I_{j_2}, \dots, I_{j_{N_t}}$. \mathbb{M}_i is a candidate model if $\exists I_{j_s} : r(\mathbb{M}_i, I_{j_s}) = 1, s = 1 : N_t$. Note that IR may identify multiple candidate models (N_m) for localizing the query image. In this case, the camera pose is estimated using the 3D model with the maximum number of 2D-3D correspondences (Section III-B). The summary of image retrieval is as follows: First, we extract SIFT features [28] and embed them into high dimensional using Triangulation Embedding (T-embedding) [27]. As a result, each image has a fixed-length T-embedding feature as a discriminative vector representation. We set the feature size to 4096. To reduce the memory requirement and improve the searching efficiency, we apply Product Quantization (PQ) with Inverted File (IVFADC) [30] to the T-embedding features. Details can be found in [30], [27]. Note that the PQ codes are compact. As a result, we can fit the entire PQ codes of 227K reference images into the RAM of a mobile device. Processing time for IR is less than 1s (GPU acceleration) for 227K reference images on a mobile device. Note that 227K images correspond to approximately 15km road distance coverage.

Using IR to index 3D models is memory efficient because only a few number of models are processed each time. However, it is more expensive by 2D-3D correspondence search due to matching between the query and N_m models. That leads to our idea of the proposed correspondence search, which aims to reduce this computational complexity.

B. Fast 2D-3D correspondence search

Our proposed method for 2D-3D correspondence search, namely Cascade Correspondence Search (CCS), consists of two parts: (i) an efficient 2D-3D matching is to seek top ranked list of nearest neighbors in cascade manner and (ii) a fast and effective RANSAC enables to exploit inliers from a large number of correspondences that helps to boost the accuracy.

1) *Cascade search for 2D-3D matching*: Our method leverages the efficient computation of Hamming distance. We follow the Pigeonhole Principle on binary code [31] to further accelerate the search. The key idea is on following [31]: A binary code \mathbf{h} , comprising d bits, is partitioned into m disjoint

sub-binary vectors, $\mathbf{h}^{(1)}, \dots, \mathbf{h}^{(m)}$, each has $\lfloor \frac{d}{m} \rfloor$ bits. For convenience, we assume that d is divisible by m . When two binary codes \mathbf{h} and \mathbf{g} differ at most r bits, then, at least, one of m sub-binary vectors, for example $\{\mathbf{h}^{(k)}, \mathbf{g}^{(k)}\}, 1 \leq k \leq m$, must differ at most $\lfloor \frac{r}{m} \rfloor$ bits. Formally, it can be written:

$$\|\mathbf{h} - \mathbf{g}\|_H \leq r \Rightarrow \exists k \in [1, m] : \|\mathbf{h}^{(k)} - \mathbf{g}^{(k)}\|_H \leq \lfloor \frac{r}{m} \rfloor \quad (1)$$

where $\|\cdot\|_H$ is the Hamming distance. We apply it to our context of 2D-3D matching and propose additions and improvements:

- In our work, since the 3D models are built off-line and SIFT descriptors for 3D points are available during off-line processing, we propose to train a data-dependent hash function to improve matching accuracy.
- We use a single hash function for mapping from 128 bytes SIFT to d bits binary vector. Splitting the long d bits code into m short codes of b bits to construct m lookup tables (LUT) for coarse search and use full d bit vector for the refined search.
- We add the precise search layer to the hashing scheme and propose to use Product Quantization (PQ) [30], a fast and memory efficient method for precise search. Consequently, our work combines hashing and PQ in a single pipeline to leverage their strengths: Binary hash code enables fast indexing via Hamming distance-based comparison, while PQ achieves better matching accuracy. They are both compressed descriptors.
- We propose to use a prioritizing scheme based on the number of candidates resulted from coarse search layer. Results show that this scheme significantly accelerates about $\sim 10\times$ with only slightly less accuracy. The valuation is demonstrated on Dubrovnik dataset in Table IV.

The pipeline of our proposed 2D-3D matching method is shown in Fig. 9. The method includes three main steps: coarse search, refined search, and precise search. Two first steps are to quickly filter out a shorter list of candidates from N_p 3D points' descriptors, the last step to precisely determine the top-ranked list. Let $d = 128$ be the feature dimension of SIFT descriptors. Given a 3D model and its points' descriptors, each descriptor $\mathbf{d} \in \mathbb{R}^{d \times 1}$ are pre-mapped into binary vector \mathbf{h} in Hamming space $\mathbb{B}^{d \times 1}$: $\mathbf{h} = \text{sign}(\mathbf{W}\mathbf{d})$, where \mathbf{W} is the transformation matrix, which can be learned via objective minimization:

$$\arg \min_{\mathbf{W}, \mathbf{H}} \|\mathbf{H} - \mathbf{W}\mathbf{D}\|_F^2 \quad (2)$$

where $\|\cdot\|_F$ is Frobenius norm. \mathbf{D}, \mathbf{H} are matrices of all point descriptors of 3D model (one descriptor per matrix's column) and its binarized code after transformation respectively. We solve the optimization problem by ITQ [32]. Given the learned hash function, all descriptors of the model are mapped into binary vectors and we store those vectors instead of original SIFT descriptors.

Coarse search: We follow the principle (1) to create a LUT based data structure for fast search. We split binary vector \mathbf{h}

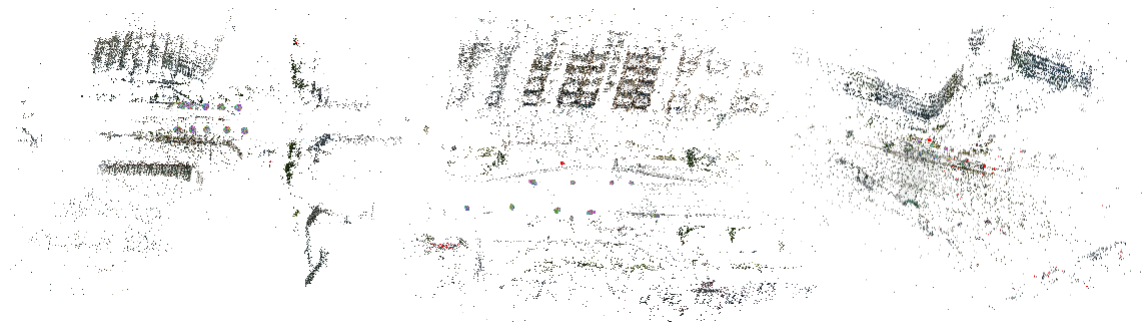


Fig. 7. Examples of 3D models reconstructed by SfM.

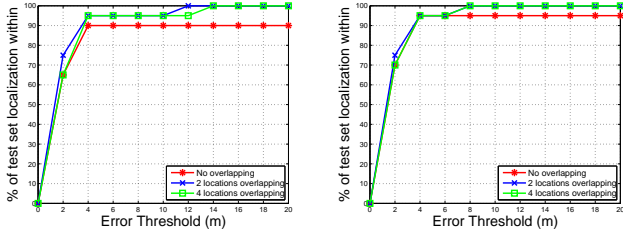


Fig. 8. The number of overlapped placemarks of two segments, and its effects on the image-retrieval top list of 20 or 50. Two placemarks can ensure good localization accuracy. The retrieved list of 20 database images achieves good accuracy-speed trade-off.

TABLE II
THE TRADE-OFF BETWEEN THE NUMBER OF CANDIDATES \mathbf{L}_C AND THE SIZE OF LUT EXPERIMENTED ON DUBROVNIK DATASET.

Method(m, b)	\mathbf{L}_C	LUT size
ITQ(4,32)	-	$4 \times 2^{32} \times 4 = 64\text{GB}$
ITQ(8,16)	$\sim 5K$	$8 \times 2^{16} \times 2 = 1048KB$
ITQ(16,8)	$\sim 60K$	$16 \times 2^8 = 4096B$
LSH(8,16)	$\sim 20K$	$8 \times 2^{16} \times 2 = 1048KB$

into m sub-vectors $\{\mathbf{h}^{(k)}\}, k \in [1 : m]$ of b bits ($m \cdot b = d$). In our work, we only select candidates differ at most $r = m - 1$ bits from the query ($\lfloor \frac{r}{m} \rfloor = 0$). In other words, a candidate's binary vector is potentially matched to the query's iff at least one of their sub-vectors are exactly the same. For training, we create m LUTs, where $\mathbf{LUT}^{(k)}$ for the sub-vector $\mathbf{h}^{(k)}$, and each LUT comprises of $K_b = 2^b$ buckets. One bucket links to a point-id list of 3D points that are assigned to buckets according to their binary sub-vectors. For searching, a query descriptor is first mapped into Hamming space and was divided into m sub-binary vectors as above. And then looking up into the $\mathbf{LUT}^{(k)}$ to find a certain bucket that matches the binary code of $\mathbf{h}^{(k)}$. This results in the point-id list $\mathbf{L}^{(k)}$:

$$\mathbf{L}^{(k)} = \mathbf{LUT}^{(k)}(\mathbf{h}^{(k)}), k = 1, \dots, m \quad (3)$$

Then, merging m point-id list to have the final list of coarse search $\mathbf{L}_C = [\mathbf{L}^{(1)}, \dots, \mathbf{L}^{(m)}]$. By using LUT, the search complexity of $\mathbf{h}^{(k)}$ is constant $O(1)$ to retrieve the point-id list $\mathbf{L}^{(k)}$. This step results in a short list \mathbf{L}_C contains $|\mathbf{L}_C|$ candidates for the next search. It is important to choose appropriate values of m and b to the trade-off between the memory requirement of LUT and computation time (which

depends on the length of \mathbf{L}_C that requires Hamming distance refining). As shown in Table II, we map descriptors to binary codes by using ITQ with different settings and also replace it with LSH [33]. ITQ($m = 4, b = 32$) is impractical due to over-large size requirement of LUTs. ITQ($m = 16, b = 8$) results in too many candidates, which slows down the refined search. ITQ($m = 8, b = 16$) is the best option, results in the short list, and requires a small amount of LUT memory (excluding the overhead memory of descriptors indexing). Using LSH results in the longer list ($\sim 4 \times$ of ITQ) of candidates, which means that learning the hash mapping from data points by ITQ is more efficient than a random method LSH in our case. This is consistent with our experiments conducted later in Fig. 13.

Refined search: In this step, we use full d -bit code \mathbf{h} to refine \mathbf{L}_C list to pick out a shorter list \mathbf{L}_R ($|\mathbf{L}_R| \leq 50$). First, we compute exhaustively the Hamming distance between the d -bit code of query to that of \mathbf{L}_C candidates. Then, candidates are re-ranked according to these distances. Computing Hamming distance is efficient because we can leverage low-level machine instructions (XOR, POPCNT). Computing Hamming distance of two 128-bit vectors is significantly faster ($\geq 30 \times$) than the Euclidean distance of SIFT vectors and accelerate ($\geq 4 \times$) ADC [30] on our machine. Furthermore, Hamming distance of d -bit code has the limited range of $[0, 128]$, which allows us to build the online LUT during the refined search. By this way, selecting top candidates \mathbf{L}_R search is accelerated. However, the limited range prevents us to precisely rank candidates. That leads to the last step of our pipeline.

Precise search: The purpose of the precise search is to get \mathbf{L}_R ranked better so that we can choose the best candidate or remove outliers of matches before applying geometric verification. Furthermore, we can consider their order as an useful prior information. It plays an important role to reduce the complexity of pose estimation (discussed in Section of Geometric Verification). The approximated Euclidean distance by ADC of PQ [30] is used. The match between a query feature and a 3D point is established if the distance ratio from the query to the first and second candidates passes the ratio test ν_h [28]; otherwise, rejected as outliers. The sub-quantizers of PQ are trained once from an independent dataset, SIFT1M [28], and used in all experiments. In this step, we need to store PQ codes in addition to hashing code of two previous steps.

Prioritization: Finding all matches between 2D features and 3D points to infer camera pose is expensive because the

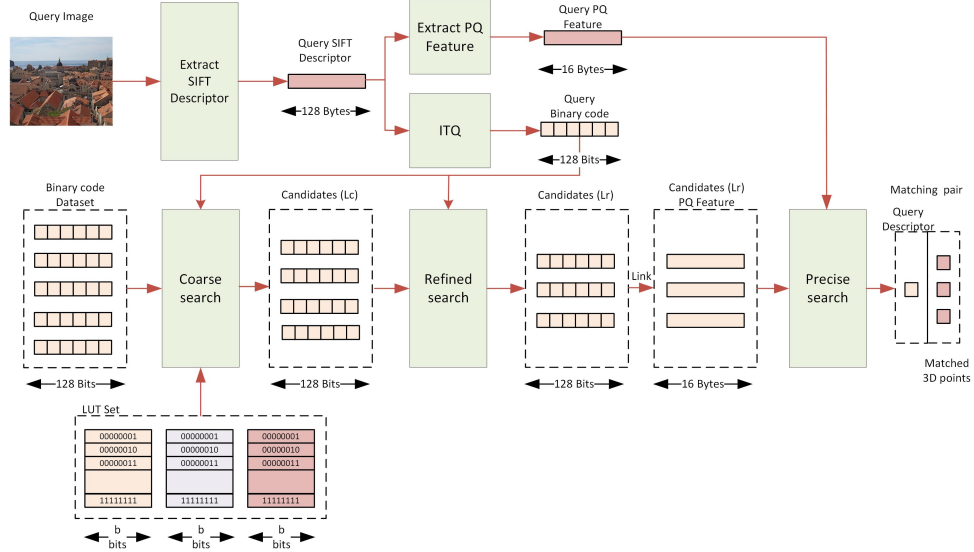


Fig. 9. The pipeline of our cascade search per one query descriptor. It consists of three main steps: coarse search (16-bit LUT), refined search (128-bit) and precise search (16-byte).

query image can contain thousands of features. In practice, the method can early stop once found a sufficient number of matches [22]. Therefore, we perform a prioritized search on descriptors of the 2D image as follows: given a query descriptor, the coarse search returned the point-id list \mathbf{L}_C . We first continue the refined and precise search with those query features having shorter list $|\mathbf{L}_C|$. A correspondence is established if the nearest candidate passes the ratio test with threshold ν_h on precise search. We stop the search once $N_{early} = 100$ correspondences have been found.

2) *Geometric verification*: After 2D-3D matching, one query descriptor has one 3D point correspondence. Those correspondences (one-one matches) is then verified by RANSAC within 6-MLT algorithm inside. Empirically, we found two things: (i) ratio test ν_h tends to reject many good matches (ii) good candidates are not always highest-ranked in the list \mathbf{L}_R . It is probably due to repetitive features in buildings, that is a common issue of localization in urban environment [3], [24]. Therefore, relaxing the threshold to accept more matches, and filtering wrong matches by using geometric verification seems a potential solution. Recent works [2], [24] aim to approach this way, but their geometric solvers are too slow for practical applications.

To address this issue, we propose a fast and effective RANSAC as follows: First, we relax the threshold $\nu > \nu_h$ to accept more matches and keep one-many candidates per query descriptor. We compute one-many matchings: given one query feature, we accept M top candidates in \mathbf{L}_R list when $d_0/d_1 < \nu$. d_0 and d_1 are the first and second smallest distances of the query to \mathbf{L}_R candidates. However, processing all these matchings leads to an exponential increase in computational time in RANSAC due to a very low rate of inliers. We avoid this issue by considering its subset to generate the hypothesis. As consequence, we propose two different sets of matchings in the hypotheses and verification stages of RANSAC. The first set contains the one-one (1-1) matchings that pass a ratio test

with threshold ν_h . The second set of candidates found by the relaxed threshold, and contains one-many (1- M) matchings as mentioned above. We propose to use the first set to generate hypotheses and the second set for verification. We found that using relaxed threshold and 1- M matchings in verification can increase the number of inliers, leading to the accuracy improvement. We further speed up our method by using the pre-verification step like [34] in the middle, to quickly reject "bad" samples before performing verification.

For detail, let $\mathbf{Q} = \{\mathbf{q}_i\}$, and $\mathbf{P} = \{\mathbf{p}_{ij}\}$, $i = 1 : N_q$, where N_q is the number of query descriptors found their matchings. \mathbf{q}_i is the 2D coordinate of i -th query and \mathbf{p}_{ij} is the 3D coordinate of its corresponding j -th ranked 3D point. Those matchings found by 2D-3D matching with the threshold ν . One query \mathbf{q}_i has many candidates (1- M) $\mathbf{P}_i = \{\mathbf{p}_{ij}, j = 1 : |\mathbf{P}_i|\}$, where $|\mathbf{P}_i|$ is the number of point candidates matched with each query \mathbf{q}_i : $|\mathbf{P}_i| \leq M$ (verification set). Without the loss of generality, \mathbf{p}_{ij} were sorted in ascendant of ADC distance to the query \mathbf{q}_i : $d(\mathbf{q}_i, \mathbf{p}_{ij})$. And among N_q 1- M matchings, assuming that there are N_h 1-1 matchings $\{\mathbf{q}_{i_k}, \mathbf{p}_{i_k1}\}$ (hypothesis set), $i_k \in [1 : N_q]$, $k = 1 : N_h$ found by the threshold ν_h . The detail of proposed algorithm is presented in Fig. 10. ϵ indicates the probability $p(1|H_g)$ that any randomly match is consistent with a "good" model. $s = 6$ indicates the minimum size of a sample can estimate the model parameters θ by using 6-MLT algorithm. δ indicates the probability $p(1|H_b)$ of a match being consistent with a "bad" model. The probability of rejecting a "good" sample ($\alpha = 1/A$). Here, H_g : the hypothesis that the model is "good", and H_b : the alternative hypothesis that the model is "bad". $\rho_1(\theta, \cdot)$ and $\rho_M(\theta, \cdot) \in \{0, 1\}$ are functions to evaluate whether 1-1 matches or 1- M matches are consistent with the model or not. $\rho_M(\theta, \{\mathbf{q}_i, \mathbf{p}_{ij}\}) = 1$ if $\exists k, \rho_1(\theta, \{\mathbf{q}_i, \mathbf{p}_{i_k1}\}) = 1$. C and θ are the cost (or the number of inliers) and model parameters respectively. The adaptive decision threshold $A = A(\delta, \epsilon)$ is computed similarly as [34].

```

1: procedure CCS-RANSAC( $\mathbf{Q}, \mathbf{P}, \{i_k\}_{k=1}^{N_h}$ )
2:    $\epsilon \leftarrow p(1|H_g) = \frac{s}{N_h}$ 
3:    $\delta \leftarrow p(1|H_b) = 0.01$ 
4:    $A \leftarrow A(\delta, \epsilon)$ 
5:    $\mu \leftarrow \frac{1}{\epsilon^m * (1 - \frac{1}{A})}$ 
6:    $nr \leftarrow 0$  ▷ the number of rejected times
7:    $iter \leftarrow 0$  ▷ the number of iterations
8:   while  $iter \leq \mu$  do
9:      $iter \leftarrow iter + 1$ 
10:    I. Hypothesis
11:    Select a random sample of minimum size  $s$  from hypothesis set
12:     $\{\mathbf{q}_{i_k}, \mathbf{p}_{i_{k+1}}\}, i_k \in [1 : N_q], k = 1 : N_h$ .
13:    Estimate model parameters  $\theta$  fitting the sample.
14:    II. Pre-verification
15:     $k = 1$ 
16:     $\lambda_0 = 1$ 
17:    while  $k \leq N_h$  do
18:      Let  $\rho_1 \leftarrow \rho_1(\theta, \{\mathbf{q}_i, \mathbf{p}_{i1}\})$  ▷ 0 or 1
19:       $\lambda_k \leftarrow \lambda_{k-1} * (\rho_1 * \frac{\delta}{\epsilon} + (1 - \rho_1) * \frac{1-\delta}{1-\epsilon})$ 
20:      if  $\lambda_k > A$  then
21:         $bad\_model = true$  ▷ Reject sample
22:        break
23:      else
24:         $k \leftarrow k + 1$ 
25:      end if
26:    end while
27:    if  $bad\_model$  then
28:       $nr \leftarrow nr + 1$ 
29:       $\hat{\delta} \leftarrow \delta * \frac{nr-1}{nr} + \epsilon * nr$  ▷ Re-estimate  $\delta$ 
30:      if  $|\delta - \hat{\delta}| > 0.05$  then
31:         $\delta \leftarrow \hat{\delta}$  ▷ Update  $\delta$ 
32:         $A \leftarrow A(\delta, \epsilon)$  ▷ Update  $A$ 
33:      end if
34:    continue
35:    III. Verification
36:    Compute cost  $C \leftarrow \sum_i \rho_M(\theta, \{\mathbf{q}_i, \mathbf{p}_i\})$ 
37:    if  $C^* \leq C$  then
38:       $C^* \leftarrow C, \theta^* \leftarrow \theta$  ▷ Update good model
39:       $\epsilon \leftarrow C^* * \frac{l_R}{N_q}$  ▷ Update  $\epsilon$ 
40:       $A \leftarrow A(\delta, \epsilon)$  ▷ Update  $A$ 
41:       $\mu \leftarrow \frac{1}{\epsilon^m * (1 - \frac{1}{A})}$  ▷ Update  $\mu$ 
42:    end if
43:  end while
44: end procedure

```

Fig. 10. The algorithm of our proposed RANSAC.

IV. EXPERIMENTAL RESULTS

We conduct experiments to validate our CCS method and the overall system. Specifically, we adopt four benchmark datasets: Dubrovnik [9], Rome [9], Vienna [21], and Aachen [35], to evaluate our correspondence search method and compare to the state of the art. Table III provides some information about these datasets. Then, we investigate our on-device system, which trained from our dataset of 227K images, by using 576 mobile queries for IR and localization. Experiments are conducted on our workstation: Intel Xeon Octa-core CPU E5-1260 3.70GHz, 64GB RAM, and Nvidia Tablet Shield K1. We use “mean descriptors” of each 3D point in all experiments. We have different settings of our method: Setting 1 indicates our method with traditional RANSAC, Setting 2 indicates uses new 1-M RANSAC scheme. Setting 3 indicates our method with new RANSAC and prioritizing scheme included.

TABLE III
STANDARD DATASETS FOR THE EVALUATION OF 2D-3D
CORRESPONDENCES SEARCH.

Dataset	#Cameras	#3D Points	#Descriptors	#Queries
Dubrovnik	6044	1,886,884	9,606,317	800
Rome	15,179	4,067,119	21,515,110	1000
Aachen	3047	1,540,786	7,281,501	369
Vienna	1324	1,123,028	4,854,056	266

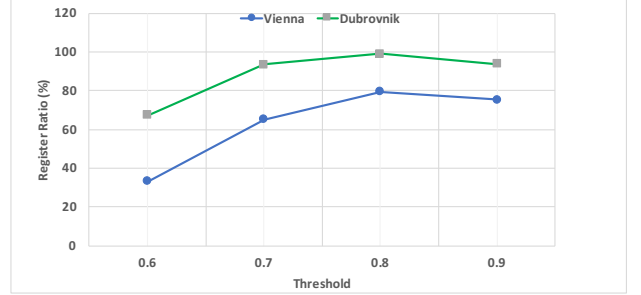


Fig. 11. Studying the influence of test ratio thresholds on Dubrovnik and Vienna datasets. This experiment determines the good ratio threshold for precise search. Results show that threshold $\nu_h = 0.8$ achieves the highest registration rate. In the figure, the horizontal axis indicates the value of thresholds, and the vertical axis indicates the percentage of registered images.

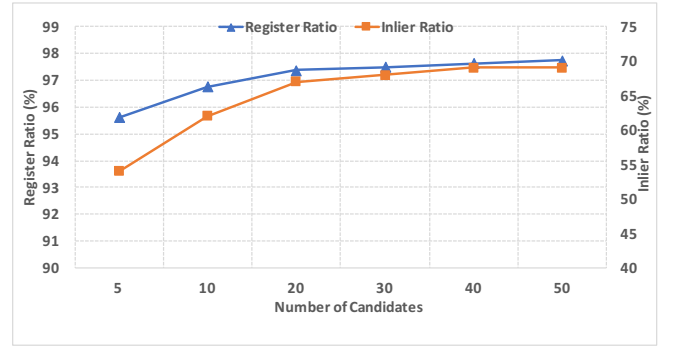


Fig. 12. The registration rate and inliers ratio according to the number of candidates of \mathbf{L}_R .

A. Hashing based 2D-3D matching

The first experiment is to determine a good test ratio threshold for precise search. It is conducted on Dubrovnik and Vienna datasets. We use ADC with Inverted File [30] with the number of coarse quantizer $K_c = 256$, 16 sub-vectors of SIFT, the number of sub-quantizers $K_{pq} = 2^8$, and the number of neighboring cells visited $w = 8$. We use small K_c and large w to ensure that quantization does not significantly affect the overall performance. In this experiment, we fix 5000 iterations to attain the same probable result in multiple runs with RANSAC. A query image is “registered” if at least twelve inliers found, same as [9]. This experiment suggests the threshold $\nu_h = 0.8$ is a good option, Fig. 11.

The second experiment to choose the good size of $|\mathbf{L}_R|$ output from refined search. Conditions like the first experiment, except we choose the best threshold $\nu_h = 0.8$ for precise search. We validate our method with a various number of candidates in \mathbf{L}_R . This experiment suggests that $|\mathbf{L}_R| = 40$

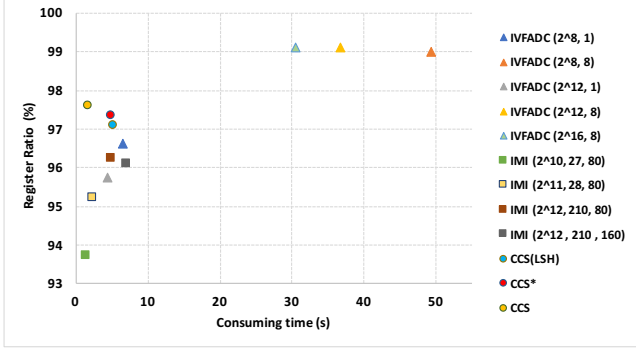


Fig. 13. Comparison on indexing methods for PQ. Parameters for IVFADC (K_c, w), IMI ($K_c, w, |\mathbf{L}_R|$), CCS ($K_b = 2^{16}, |\mathbf{L}_R| = 40$). The version of our CCS is Setting 1, and '*' indicates our CCS ignoring the refined search.

is a good option because increasing it does not significantly affect the registration rate and inliers ratio (Fig. 12).

In the third experiment on Dubrovnik dataset, we study the influence of different indexing procedures on accuracy and computation, by comparing our method to two well-known PQ-based indexing schemes. Conditions like the second experiment, we compare our CCS to Inverted File (IVFADC) [30], Inverted Multi-Index (IMI) [25]. We also compare to ourselves without refined search. We tune parameters of IVFADC and IMI for a fair comparison. Results in Fig. 13 demonstrate the efficiency of refined search, because removing this step slowing down CCS about $\sim 3\times$, though obtaining the similar registration rate. IVFADC with $w = 8$ visited cells achieves highest performances with different sizes of sub-quantizers, but it is too slow. Our method outperforms IVFADC (with $w = 1$) at both execution time and registration rate. IMI registers more queries when increasing the number of nearest neighbors w or the length of its re-ranking list \mathbf{L}_R (same meaning as ours). Yet it also increases processing time. Our registration rate is higher than IMI, while our running time is competitive. We try to replace ITQ by LSH [33] in our same hashing scheme. Results show that using ITQ is $\sim 3\times$ faster than LSH. This is consistent with the parameter of the number of candidates reported in Fig. 13. Note that all experiments above, we use 1-1 matchings and traditional RANSAC (Setting 1).

B. Pose estimation and prioritization

In this section, we investigate the influence of our geometric verification (Setting 2), that combines cascade search and proposed RANSAC with a fixed number of 5000 iterations. We visualize the inliers found by our method on Dubrovnik dataset to understand the impact of the ratio test. We adopt all candidates of \mathbf{L}_R , $M = |\mathbf{L}_R|$, in this experiment. Fig. 14 The number of inliers per query on Dubrovnik (first row) and Vienna (second row) datasets. Left figures show the number of inliers (on first 70 queries of Dubrovnik/Vienna) found by threshold $\nu_h = 0.8$ (blue), and relaxed threshold $\nu = 0.9$ (red). Right figures are the percentage of number inliers contributed by candidates (from second order) in the list \mathbf{L}_R . On Vienna dataset, we increase approximately 100% of inliers as using

relaxed threshold and contribute about nearly 48% to the total of the number of inliers. The candidate list on Vienna dataset contributes a slightly higher number of inliers than on Dubrovnik dataset. These explain why our method achieves better results on Vienna dataset. Fig. 15 shows inliers on one query example of Dubrovnik. For each query, the blue part is the number of inliers found by the strict ratio ν_h , and the red part is the additional ones found by the relaxed threshold ν . In average, the relaxed threshold can increase about 65.4% of inliers from the strict threshold, and contributes about 37.2% to the total number of inliers found by our method (Setting 2). The right-hand-side of the first row is the average number of inliers contributed by 1- M matchings (from the second rank). The 1- M matches increase about average 15% of the number of inliers from the strict threshold of 1-1, and about 7% of the total. It means if we use ν threshold and 1- M matchings, the method increase a significant number of inliers ($\geq 80\%$). We see on the right figure that lower ranked candidates < 5 -th does not have the significant impact on the total number of inliers; therefore to save the computation, we keep only $M = 5$ matchings after the precise search.

Table IV demonstrates the performance of our Setting 2 ($M = 5$). First, we see that our Setting 2 really outperforms our Setting 1 at both the number of registered images and errors. It confirms that using relaxed 1- M candidates per query improves the performance. The registration rate and running time of Setting 2 is competitive to the state of the art, however, its processing time can be further reduced by leveraging prioritizing scheme. We improve the cascade search speed with prioritized scheme (Setting 3). In the same Table IV, Setting 3 obtains similar performance as the full search but is about $\sim 7\times$ faster. By prioritizing scheme, we achieve the similar accuracy but accelerate matching much faster than previous works. We also perform comparison using other standard datasets (Table V). Our Setting 3 outperforms the state-of-the-art methods in registration rate on Vienna and Aachen datasets. In addition to that, our proposed method is more efficient with regards to memory because of the use of compressed descriptors. Note that when possible, we run the 2D-3D matching methods on our machine and measure their running time (excluding RANSAC time). This shows the potential of using relaxed and 1- M matches for better accuracy. However, our version of Setting 3 (fixed 5000 iterations) used in above experiments can be further improved in term of execution time.

We accelerate it by using pre-verification step (Setting 3⁺). It remains competitive accuracy, but $\sim 20\times$ faster from RANSAC (5000 iterations) of Setting 3, as shown in Table VI. As a result, the total time of Setting 3 with our fast RANSAC is faster than Setting 3, and it needs totally only 0.12(s) to successfully register one query. As compared to others, we outperform them both registration rate and execution time on Vienna and Aachen datasets (Table VII). Our proposed RANSAC (Setting 3⁺) executes as fast as classical RANSAC on the small set of correspondences, e.g. 0.03(s) vs. 0.01(s) per Dubrovnik query in Table VI.

As being discussed in next section, our model can reduce the memory requirements by the factor of about $\times 2$ from

TABLE IV

WE COMPARE OUR METHOD TO THE STATE OF THE ART ON DUBROVNIK DATASET. METHODS MARKED ‘+’ REPORTS ONLY THE PROCESSING TIME OF OUTLIER REJECTION/VOTING SCHEME, TAKEN FROM ORIGINAL PAPERS (IGNORING THE EXECUTION TIME OF 2D-3D MATCHING). METHODS MARKED ‘**’ REPORT RESULTS AFTER BUNDLE ADJUSTMENT.

Method	#reg. images	Median	Quartiles [m]		#images with error		Time (s)
			1st Quartile	3st Quartile	< 18.3m	>400m	
Kd-tree	795	-	-	-	-	-	3.4*
[9]	753	9.3	7.5	13.4	655	-	
[22]	782.0	1.3	0.5	5.1	675	13	0.28
[36]	784.1	-	-	-	-	-	
[35]	786	-	-	-	-	-	
[23]	795.9	1.4	0.4	5.3	704	9	0.25
[3]	797	-	-	-	-	-	
[37]	796	-	-	-	-	-	
[24]	798	1.69	-	-	725	2	3.78 ⁺
[24]*	794	0.47	-	-	749	13	-
[2]	798	0.56	-	-	771	3	5.06 ⁺
[1]	800	-	-	-	-	-	
Setting 1	781	0.93	0.34	3.77	710	12	0.62
Setting 2	796	0.89	0.31	3.67	717	17	0.62
Setting 3	794	1.06	0.39	4.15	711	10	0.09

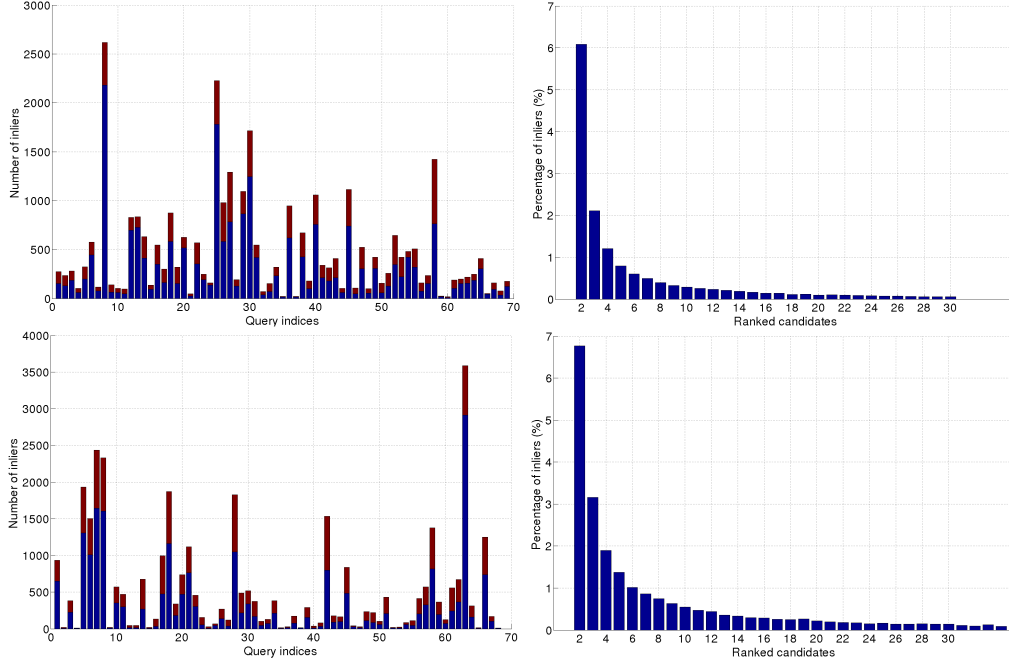


Fig. 14. The contribution of inliers (on first 70 queries of Dubrovnik and Vienna) found by threshold $\nu_h = 0.8$ (blue), and additional inliers found by relaxed threshold $\nu = 0.9$ (red).

TABLE V

THE NUMBER OF REGISTERED IMAGES ON ROME, VIENNA, AND AACHEN DATASETS.

Method	Rome	Vienna	Aachen
Kd-tree	983	221	317
[9]	924	204	-
[3]	990.5	221	318
[37]	997	-	329
[35]	984	227	327
[36]	979	-	298.5
[1]	997	-	-
Setting 2	991	241	340
Setting 3	991	236	338

TABLE VI

THE PROCESSING TIMES OF RANSAC AND THE REGISTRATION TIMES.

Method	#reg. images	RANSAC (s)	Reg. time (s)
Kd-tree	795	0.001	3.4
[22]	782.0	0.01	0.28
[23]	795.9	0.01	0.25
Setting 3	794	0.20	0.29
Setting 3⁺	793	0.03	0.12

our model to [10] for memory efficiency. We conduct this experiment on Dubrovnik model (1.8×10^5 3D points) by using [10] to compress this model by certain factors and use IVFADC (which achieved the best registration rate among compared PQ methods, Fig. 13) to obtain the registration on

the original SIFT model. In this experiment, we compare



Fig. 15. The left figure has 160 inliers found by our Setting 1 (with ν_h), and the right figure has 278 inliers found by our Setting 2 (with the relaxed threshold ν).

TABLE VII
THE RUNNING TIMES (INCLUDING RANSAC) ON VIENNA AND AACHEN DATASETS.

Method	Vienna		Aachen	
	#reg. images	Reg. time (s)	#reg. images	Reg. time (s)
[22]	206.9	0.46	-	-
[23]	220	0.27	-	-
[3]	221	0.17	318	0.12
Setting 3	236	0.35	338	0.28
Setting 3⁺	228	0.15	335	0.11

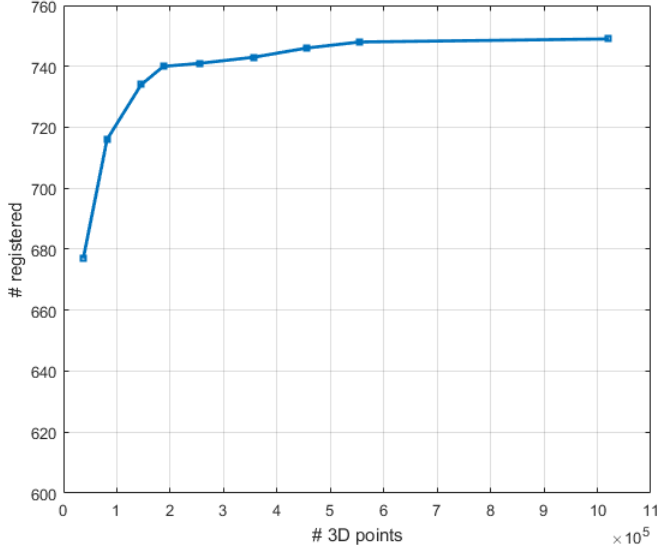


Fig. 16. The number of 3D points of compressed Dubrovnik models and the registration rate of IVFADC method on the corresponding models.

those compressed models. Fig. 16 shows that compressing Dubrovnik model to 10×10^5 3D points (about $\times 1.8$), the registration rate of IVFADC dramatically drop from 796 (99.5%) to 750 (93.75%). At similar compression factor (about $\times 2$), our method can achieve about 97.3% with Setting 1, and 99.25% with our best Setting 3.

C. On-device system

In order to evaluate our on-device system, we consider the robustness of image retrieval on a large-scale dataset and the localization accuracy of overall system on our dataset.

1) *Image retrieval*: Image retrieval in our system is to find correct 3D models that a query likely belongs to. A query

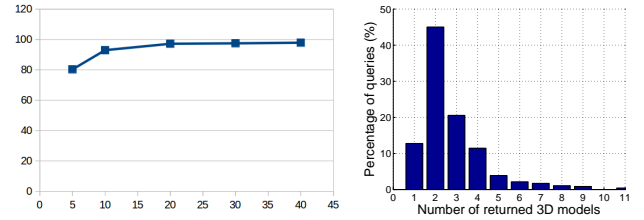


Fig. 17. The accuracy of image retrieval and the histogram of the model number of threshold 20.

image is “success”, if N_t top list of retrieval images match to *at least* one correct model. For ground-truth, we manually index our set of queries to their corresponding 3D models. It is important to investigate image retrieval performance, because it much affects the robustness of the overall system, especially with a large-scale dataset. We follow the parameters reported in T-embedding method [27] as represented above and use sum-pooling. The goal is to determine the number of retrieved image N_t should be returned from image retrieval. N_t has to balance between the accuracy and the number of models found. Fig. 17 shows that $N_t = 20$ is an appropriate number. The horizontal axis is the number of references resulted from image retrieval, and the vertical axis is the percentage of queries found at least one correct model. The histogram of model numbers is visualized on the same figure. More than 80% of queries found ≤ 4 candidate models, therefore, we practically perform 2D-3D matching with the maximum number of four models if the list results in more than this number.

2) *Overall system localization*: In this experiment, the localization accuracy is measured by GPS distance between ground-truth and our estimation. The results are drawn in form of Cumulative Error Distribution (CED) curve. The horizontal axis indicates the error threshold (in meters), and

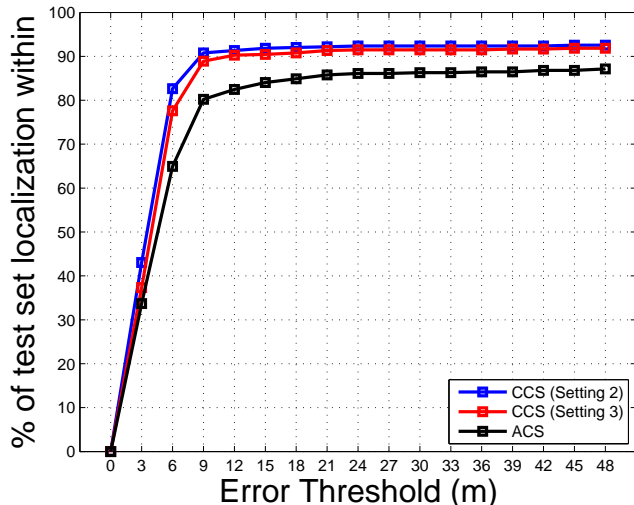


Fig. 18. The performances of the overall system tested on 576 query images using two different 2D-3D matching method ACS and our method.

the vertical axis indicates the percentage of image numbers having lower or equal errors than the threshold. We compare correspondence search methods on the system: ACS [23] and our Setting 3⁺. The same image retrieval component used for both that was trained on 227K images. Fig. 18 presents real-world accuracies, e.g. at the threshold of 9(m), about 90% queries are well-localized for our Setting 3⁺, a little worse for our Setting 3 without our fast RANSAC, and about 80% for ACS. Our CCS uses compressed SIFT descriptors, which optimized better memory requirements than ACS but achieved better performance than ACS on our dataset. Note that camera is calibrated in this experiment. About 10% of images are completely failed (≥ 50 (m)) due to image retrieval, the confusion of similar buildings, or reflection of building facades. Our proposed system achieves encouraging results using GSV images: the median error of our CCS (Setting 3⁺) is about 3.75 (m), and 72% of queries have errors less than 5 (m).

D. Mobile implementation

1) *Image retrieval*: Our vocabulary size of T-embedding is $k_{temb} = 32$, thus its T-embedding feature dimension is 4096. The fixed consumption of embedding and aggregating parameters is 67.14 (MB). The indexing step of PQ needs approximately 129.44 (MB) to encode $N = 227K$ images, where the number of sub-vectors is $g = 256$ and the number of sub-quantizer per sub-vector is 256. The total memory is 129.44 (MB), which can easily fit modern devices with RAM $\geq 1GB$. As increasing the size of a dataset to 1M images, the total memory consumption is 327.34 (MB) is still processable on the RAM.

2) *2D-3D correspondence search*: CCS (Setting 3⁺) is implemented for mobile implementation as it is fast and requires less memory. The method requires 32 bytes (128-bit (16 bytes) hash code and 16 bytes PQ code) to encode a SIFT descriptor. Using $N_l = 8$ look-up tables, each one is

TABLE VIII
MEMORY REQUIREMENTS (#BYTES) FOR OUR MODEL VS. ORIGINAL MODEL.

	Our model	Original model
Look-up tables	$8 \times 2^{16} \times 4$	-
Point id	$8 \times N_p \times 4$	$N_p \times 4$
Point coordinates	$N_p \times 12$	$N_p \times 12$
Descriptors	$N_p \times (16 + 16)$	$N_p \times 128$
Total memory	$\approx N_p \times 76$	$N_p \times 144$

comprised $K_b = 8 \times 2^{16}$ buckets. Each bucket needs a 4-byte pointer referring to one point-id list. Let N_p is the point number of the 3D model if N_p is large enough, the overhead memory is small can be ignored. N_l tables refer to N_l point-id of total N_p points. One point-id can be represented by a 4-byte integer number. N_p 3d point coordinates consume $N_p \times 12$ bytes. Our model needs the total of $N_p \times 76$ bytes, which is near $\sim 2x$ compressed than the original model (the 3D model of using SIFT descriptors) of $N_p \times 144$ bytes as Table VIII (ignoring the indexing structures of other methods that may require more memory). Our 227K images of approximately 15km road distance coverage consume about 50MB of total memory. By some calculations, it is feasible to extend to 1M images which can range about 70 (km), while consuming less than 2GB memory. We can extend further if storing 3D models on modern SD cards. It is worth noting that the overall performance for such extensions would only affect to the accuracy of image retrieval, not 2D-3D correspondence search. Also, we trained PQ sub-quantizers from the general dataset of 1M SIFT descriptors [30], which can be used for all models. The memory requirement for PQ sub-quantizers is: $256 \times 128 \times 4$ (bytes) ≈ 0.13 (MB).

Compared to two other PQ based schemes IVFADC and IMI, which require 16-byte and 24-byte codes per 3D point, whose total memory is $N_p \times 32$ and $N_p \times 48$ (bytes) respectively. Regarding our design, although our hashing scheme needs more memory, it is not critical as the size of the model is small enough to be loaded once on device memory; furthermore, all models can be stored on an external device like SD cards. Our method is more efficient than two these methods regarding trade-off between time complexity and accuracy, which was reported on Dubrovnik dataset.

3) *On-device running time*: Our system is implemented on Android device: Nvidia Tablet Shield K1, 2.2 GHz ARM Cortex A15 CPU with 2 GB RAM, NVIDIA Tegra K1 192 core Kepler GPU, 16GB storage. Our camera solution is 1920 \times 1080. Table IX reports the running time for each individual steps: feature extraction, image retrieval, 2D-3D matching, and RANSAC. Since SIFT extraction is time-consuming, it is implemented in GPU. Image retrieval is also accelerated by GPU, whereas two other components are on CPU. The processing time of image retrieval is acceptable and consistent with dataset size. Running time of 2D-3D matching is reported for only one model. On our dataset, the number of matches found is usually less than 100, hence the early stop is not useful. In this case, our method obtains similar running time as ACS. In practice, a few of models (≤ 4) are manipulated at a time and the latency of loading one model

TABLE IX
AVERAGE RUNNING TIME FOR EACH INDIVIDUAL STEP ON OUR DEVICE.

Step	Time (s)
Feature extraction (GPU)	0.67
Image retrieval (GPU)	0.82
2D-3D matching	0.55
Pose estimation	1.15

is low, about 0.04 (s). Therefore, it takes average about 10 (s) in total to localize one query. The localization and pose estimation parts are based on single CPU core, the speed of our system can be further optimized/improved with multi-core CPU and GPU in future work. Note that we calculate the codebook size $K_{qc} = \frac{N_p}{10}$ as training ACS on our own models and other parameters as the same reported in [38].

V. CONCLUSION

We present complete design of an entire on-device system for large-scale urban localization, by combining compact image retrieval and fast 2D-3D correspondence search. The proposed system is demonstrated via the dataset of 227K GSV images (with approximately 15km road segment). The scale of the system can be readily extended with our design. Experiment results show that our system can localize mobile queries with high accuracy. The processing time is less than 10s on a typical device. It demonstrates the potential of developing a practical city-scale localization system using the abundant GSV dataset.

We propose a compact and efficient 2D-3D correspondence search for localization by combining prioritized hashing technique and 1-M RANSAC. Our 1-M RANSAC can handle a large number of matches to achieve higher accuracy while maintaining the same execution time as traditional RANSAC. Our matching method requires $\sim 2x$ less memory footprint than using original models. Our matching method achieved competitive accuracy as compared to state-of-the-art methods on benchmark datasets, especially we obtained the best performance of both processing time and registration rate on Aachen and Vienna datasets.

REFERENCES

- [1] Y. Li, N. Snavely, D. Huttenlocher, and P. Fua, "Worldwide pose estimation using 3d point clouds," in *ECCV*, 2012.
- [2] L. Svrm, O. Enqvist, M. Oskarsson, and F. Kahl, "Accurate localization and pose estimation for large 3d models," in *CVPR*, 2014.
- [3] T. Sattler, B. Leibe, and L. Kobbelt, "Efficient effective prioritized matching for large-scale image-based localization," *TPAMI*, no. 99, pp. 1–1, 2016.
- [4] N. Snavely, S. M. Seitz, and R. Szeliski, "Photo tourism: Exploring photo collections in 3d," in *SIGGRAPH*, 2006.
- [5] H. Lim, S. N. Sinha, M. F. Cohen, and M. Uyttendaele, "Real-time image-based 6-dof localization in large-scale environments," in *CVPR*, 2012.
- [6] C. Arth, M. Klopschitz, G. Reitmayr, and D. Schmalstieg, "Real-Time Self-Localization from Panoramic Images on Mobile Devices," in *ISMAR*, 2011.
- [7] J. Ventura, C. Arth, G. Reitmayr, and D. Schmalstieg, "Global localization from monocular SLAM on a mobile phone," *IEEE Trans. Vis. Comput. Graph.*, vol. 20, no. 4, pp. 531–539, 2014.
- [8] S. Middelberg, T. Sattler, O. Untzelmann, and L. Kobbelt, "Scalable 6-dof localization on mobile devices," in *ECCV*, 2014.

- [9] Y. Li, N. Snavely, and D. P. Huttenlocher, "Location recognition using prioritized feature matching," in *ECCV*, 2010.
- [10] S. Cao and N. Snavely, "Minimal scene descriptions from structure from motion models," in *CVPR*, 2014.
- [11] S. Lynen, T. Sattler, M. Bosse, J. A. Hesch, M. Pollefeys, and R. Siegwart, "Get out of my lab: Large-scale, real-time visual-inertial localization," in *Robotics: Science and Systems XI, Sapienza University of Rome, Rome, Italy, July 13-17, 2015*, 2015.
- [12] C. Arth, D. Wagner, M. Klopschitz, A. Irschara, and D. Schmalstieg, "Wide Area Localization on Mobile Phones," in *ISMAR*, 2009.
- [13] D. Anguelov, C. Dulong, D. Filip, C. Frueh, S. Lafon, R. Lyon, A. Ogale, L. Vincent, and J. Weaver, "Google street view: Capturing the world at street level," *Computer*, vol. 43, no. 6, pp. 32–38, 2010.
- [14] A. L. Majdik, Y. Albers-Schoenberg, and D. Scaramuzza, "Mav urban localization from google street view data," in *IROS*, 2013.
- [15] S. L. H. Liu, T. Mei, J. Luo, H. Li, and S. Li, "Finding perfect rendezvous on the go: Accurate mobile visual localization and its applications to routing," in *ACM Multimedia*, 2012.
- [16] A. Taneja, L. Ballan, and M. Pollefeys, "Never get lost again: Vision based navigation using streetview images," in *ACCV*, 2014.
- [17] P. Agarwal, W. Burgard, and L. Spinello, "Metric localization using google street view," in *IROS*, 2015.
- [18] W. Zhang and J. Kosecka, "Image based localization in urban environments," in *International Symposium on 3D Data Processing, Visualization and Transmission*, 2006.
- [19] D. Nister and H. Stewenius, "Scalable recognition with a vocabulary tree," in *CVPR*, 2006.
- [20] A. R. Zamir and M. Shah, "Accurate image localization based on google maps street view," in *ECCV*, 2010.
- [21] A. Irschara, C. Zach, J.-M. Frahm, and H. Bischof, "From structure-from-motion point clouds to fast location recognition," in *CVPR*, 2009.
- [22] T. Sattler, B. Leibe, and L. Kobbelt, "Fast image-based localization using direct 2d-to-3d matching," in *ICCV*, 2011.
- [23] —, "Improving image-based localization by active correspondence search," in *ECCV*, 2012.
- [24] B. Zeisl, T. Sattler, and M. Pollefeys, "Camera pose voting for large-scale image-based localization," in *ICCV*, 2015.
- [25] A. Babenko and V. S. Lempitsky, "The inverted multi-index," in *CVPR*, 2012.
- [26] D. M. Chen, G. Baatz, K. Koser, S. S. Tsai, R. Vedantham, T. Pylvanainen, K. Roimela, X. Chen, J. Bach, M. Pollefeys, B. Girod, and R. Grzeszczuk, "City-scale landmark identification on mobile devices," in *CVPR*, 2011.
- [27] H. Jégou and A. Zisserman, "Triangulation embedding and democratic aggregation for image search," in *CVPR*, 2014.
- [28] D. G. Lowe, "Distinctive image features from scale-invariant keypoints," *Int. J. Comput. Vision*, 2004.
- [29] C. Wu, "Towards linear-time incremental structure from motion," in *3DTV*, 2013.
- [30] H. Jégou, M. Douze, and C. Schmid, "Product quantization for nearest neighbor search," *IEEE TPAMI*, vol. 33, no. 1, pp. 117–128, 2011.
- [31] M. Norouzi, A. Punjani, and D. J. Fleet, "Fast search in hamming space with multi-index hashing," in *CVPR*, 2012, pp. 3108–3115.
- [32] Y. Gong and S. Lazebnik, "Iterative quantization: A procrustean approach to learning binary codes," in *CVPR*, 2011.
- [33] M. S. Charikar, "Similarity estimation techniques from rounding algorithms," in *STOC*, ser. STOC '02, 2002.
- [34] O. Chum and J. Matas, "Optimal randomized ransac," *IEEE TPAMI*, vol. 30, no. 8, pp. 1472–1482, 2008.
- [35] T. Sattler, T. Weyand, B. Leibe, and L. Kobbelt, "Image retrieval for image-based localization revisited," in *BMVC*, 2012.
- [36] Y. Feng, L. Fan, and Y. Wu, "Fast localization in large-scale environments using supervised indexing of binary features," *IEEE Trans. Image Processing*, vol. 25, no. 1, pp. 343–358, 2016.
- [37] S. Cao and N. Snavely, "Graph-based discriminative learning for location recognition," in *CVPR*, 2013.
- [38] T. Sattler, M. Havlena, F. Radenovic, K. Schindler, and M. Pollefeys, "Hyperpoints and fine vocabularies for large-scale location recognition," in *ICCV*, 2015.